

# Pre-Lithiation of Silicon Anodes by Thermal Evaporation of Lithium for Boosting the Energy Density of Lithium Ion Cells

Egy Adhitama, Frederico Dias Brandao, Iris Dienwiebel, Marlena M. Bela, Atif Javed, Lukas Haneke, Marian C. Stan, Martin Winter, Aurora Gomez-Martin,\* and Tobias Placke\*

Silicon (Si) is one of the most promising anode candidates to further push the energy density of lithium ion batteries. However, its practical usage is still hindered by parasitic side reactions including electrolyte decomposition and continuous breakage and (re-)formation of the solid electrolyte interphase (SEI), leading to consumption of active lithium. Pre-lithiation is considered a highly appealing technique to compensate for active lithium losses. A critical parameter for a successful pre-lithiation strategy by means of Li metal is to achieve lithiation of the active material/composite anode at the most uniform lateral and in-depth distribution possible. Despite extensive exploration of various pre-lithiation techniques, controlling the lithium amount precisely while keeping a homogeneous lithium distribution remains challenging. Here, the thermal evaporation of Li metal as a novel pre-lithiation technique for pure Si anodes that allows both, that is, precise control of the degree of pre-lithiation and a homogeneous Li deposition at the surface is reported. Li nucleation, mechanical cracking, and the ongoing phase changes are thoroughly evaluated. The terms dry-state and wet-state pre-lithiation (without/ with electrolyte) are revisited. Finally, a series of electrochemical methods are performed to allow a direct correlation of pre-SEI formation with the electrochemical performance of pre-lithiated Si.

E. Adhitama, F. Dias Brandao, I. Dienwiebel, M. M. Bela, A. Javed, L. Haneke, M. C. Stan, M. Winter, A. Gomez-Martin, T. Placke MEET Battery Research Center Institute of Physical Chemistry University of Münster Corrensstr. 46, 48149 Münster, Germany E-mail: agomezma@uni-muenster.de; tobias.placke@uni-muenster.de E. Adhitama, A. Javed International Graduate School for Battery Chemistry Characterization, Analysis Recycling and Application (BACCARA) University of Münster Corrensstr. 40, 48149 Münster, Germany M. Winter Forschungszentrum Jülich GmbH, IEK-12 Helmholtz Institute Münster Corrensstr. 46, 48149 Münster, Germany

The ORCID identification number(s) for the author(s) of this article can be found under https://doi.org/10.1002/adfm.202201455.

© 2022 The Authors. Advanced Functional Materials published by Wiley-VCH GmbH. This is an open access article under the terms of the Creative Commons Attribution License, which permits use, distribution and reproduction in any medium, provided the original work is properly cited.

DOI: 10.1002/adfm.202201455

#### 1. Introduction

The exploration of the true potential of lithium ion batteries (LIBs) is constantly increasing as it is one of the main drivers to a decarbonized society and renewable energy transition.<sup>[1]</sup> To increase the energy density of current LIBs to meet future energy demands, for example, for electro-mobility, there is a great interest to turn from the conventional intercalation/insertion mechanism in today's graphite-based LIBs technology toward the "alloying" mechanism with silicon (Si) which is regarded as the most promising anode material<sup>[2]</sup> (it should be noted that the formation of defined stoichiometric intermetallic phases of Li with numerous Li storage metals, such as Al, Sn, Ge, Si, etc.<sup>[3]</sup> is most often called "alloying" in the relevant battery science literature). Besides the outstanding electrochemical properties such as high gravimetric capacity (up to 3579 mAh g<sup>-1</sup>), low average de-lithiation potential (≈0.4 V vs Li|Li<sup>+</sup>), low voltage hysteresis, and thus high energy efficiency,[4]

Si features further favorable material characteristics as it is the second most abundant element in earth's crust and is environmentally benign.<sup>[5]</sup>

Nevertheless, the nature of alloys such as  $\text{Li}_x \text{S}i_v$  suffers from a large volume expansion during battery operation leading to mechanical degradation, which induces a loss of active material (e.g., contact loss or particle detachment) and thus continuously exposes the highly reactive surface to the electrolyte. [6] This is a major cause of continuous active Li losses since the trapped Li are enclosed within the pulverized materials.[7] It occurs even in the first few cycles which is indicated by drastic capacity fading. The severe mechanical fluctuation also leads to the continuous growth of the solid electrolyte interphase (SEI), which is most likely disjointed and (re-)formed in a dynamic process, causing further active lithium consumption and electrolyte decomposition upon cycling.[8] On the cell level, the severe expansion of the whole electrode might lead to penetration of the separator or even bending of the whole cell, increasing safety risks. This serious challenge necessitates stringent safety precautions to prevent any cell failure and extend the shelf life at the same time. [5b,9]

Several strategies have been proposed to alleviate such challenges toward a practical implementation, for example, by the advanced design of Si particles, [10] development of electrolyte

FUNCTIONAL MATERIALS

www.afm-iournal.de

for effective SEI formation,[11] and improvement of the electrode (e.g., by the development of novel binder systems).[11c,12] However, the exacerbation of huge volume expansion is still inevitable. Further efforts have been reported by conducting the pre-lithiation technique, which rather than dealing with volume expansion, is aimed at compensating for active lithium losses. In this respect, the pre-formed SEI, which is induced by prelithiation in combination with already partially lithiated active materials will eventually improve the cell's cycle life.[13] Prelithiation can be described as a technique to store a certain amount of active lithium in the electrode prior to battery cell operation.[13a,14] Of note, it is highly important to point out that the Li amount has to be adjusted with precise accuracy to prevent over-lithiation by considering a suitable "safety factor" for the negative electrode, as reported by Chevrier et al.[13b] With respect to the negative electrodes, several pre-lithiation techniques have already been explored namely chemical prelithiation, [15] electrochemical pre-lithiation, [16] and direct contact pre-lithiation.[17] Each technique has its specific benefits and drawbacks, especially when considering its suitability toward mass production and implementation into state-of-the-art manufacturing processes.[13a,18]

Chemical pre-lithiation opens up the possibility to control the Li amount precisely by adjusting the reaction time. However, the utilized active reagents and reaction conditions seem to introduce challenges in handling due to their rather high reactivity. Alternatively, electrochemical pre-lithiation is a simpler technique and already established in lab-scale research (i.e., by using a Li metal counter electrode), as it is close to the existing formation LIB technology. In addition, electrochemical pre-lithiation also can be performed via electrolysis of low-cost lithium salts, such as lithium chloride. [5b] Both these electrochemical pre-lithiation techniques might even be realized within roll-to-roll manufacturing processes, however, still face various challenges for practical implementation, which for example includes highly demanding conditions (e.g., additional washing and/or drying steps, optimized electrolytes) to guarantee homogeneous pre-lithiation, effective SEI formation, and high safety during manufacturing. [5b] On the other hand, the technique that is the most commonly used pre-lithiation technique reported in the literature for LIBs is direct contact pre-lithiation by using passivated Li metal powder as a Li source. [17b,19] The main benefit of this method is that the degree of pre-lithiation can be controlled with higher accuracy. Moreover, no additional step is needed because in an ideal case Li metal powder is dissolved completely prior to battery cell operation. However, besides huge concerns regarding the safety in terms of handling Li metal powder, the major drawbacks of this method are inhomogeneous lateral and in-depth Li distribution leading to challenges with non-uniform SEI formation. [17c] From the redox potential perspective, ensuring a sufficiently high homogeneity of Li distribution is critical since it ensures a homogeneous alloying reaction. If the Li distribution is inhomogeneous, the reaction appears unevenly since there might be local spots where it is lithiated and there are locations where it is not, giving rise to potential discrepancies within the electrodes. The instability of this situation (due to many variations of lithiated spot and non-lithiated spot) induces pseudo-driving force for their self-discharge and unintentional aging behavior.<sup>[13a,20]</sup>

Further, when pre-lithiation reaches maximum Si capacity, highly uniform Li distribution will induce homogeneous Li<sub>15</sub>Si<sub>4</sub> phase formation and shift the potential level of Si anodes close to the potential level of Li. Therefore, the open-circuit voltage (OCV) will likely be close to 0 V versus Li|Li+. The condition where the anode output voltage is lower than ≈1.0 V is typically the condition for electrolyte reduction.<sup>[21]</sup> The electrolyte then decomposes and an SEI layer is formed. This is a vivid method to create an SEI before the battery cells are assembled. Hence, we introduce this term as "pre-SEI formation." Normally, battery cells (e.g., conventional LiNi<sub>x</sub>Mn<sub>y</sub>Co<sub>z</sub>O<sub>2</sub> (NMC-xyz)||Si/ graphite cells) are always assembled in the fully discharged state, and the active Li content is stored within the positive electrode (cathode). During the 1st charge of the cell, the formation of the SEI at the negative electrode (anode) will consume Li+ ions from the cathode, thus decreasing the amount of active Li content within the cell and leading to capacity loss. With pre-SEI formation, these complications could be prevented as Li<sup>+</sup> ions in the cathode will not be sacrificed for forming SEI.

In this work, a novel pre-lithiation technique for Si thin films by Li thermal evaporation is reported for the first time. This pre-lithiation technique facilitates uniform Li distribution and thus homogeneous (pre-)SEI formation at the anode. The presented pre-lithiation strategy overcomes the current limitations of the previously-mentioned pre-lithiation techniques, that is, by the ability to precisely control the degree of prelithiation and a highly homogeneous Li metal deposition at the electrode surface. This study contributes as a foundation of the next level understanding of Li<sub>r</sub>Si<sub>v</sub> phase change in regard to the pre-lithiation, SEI formation, and the avoidance of Li loss during cycling in a wider sense. The Li nucleation phenomena and subsequent multi-step phase transformations caused by vapor-deposited Li are deeply investigated by varying the degree of pre-lithiation. The impact of the addition of the typical carbonate-based liquid electrolyte<sup>[22]</sup> on the reaction mechanism is explored, so the terms "dry-state" and "wet-state" pre-lithiation are revisited. Finally, an electrochemical characterization to validate active lithium losses which allows a direct correlation of an effective SEI formation to the Li distribution is performed. These phenomena are comprehensively studied for amorphous Si thin films to prevent binder and conductive carbon interference in data interpretation.[23]

## 2. Results and Discussion

# 2.1. Li Deposition Using Li Thermal Evaporation Technique: Pre-Lithiation of Si Electrodes in Dry-State

Pure amorphous (a-) Si thin films (thickness:  $\approx 300~\mu m$ ) deposited on dendritic copper foil via magnetron sputtering were used as model electrodes to directly investigate the impact and reaction mechanisms of the proposed pre-lithiation approach. The possibility to deposit Li metal using a physical vapor deposition (PVD) method namely "Li thermal evaporation" was explored (see Figure S1, Supporting Information). Li metal foil was used as the Li source with precise control depending on the desired thickness. By increasing the temperature inside an ultra-high vacuum chamber (for further details, check the

www.afm-journal.de

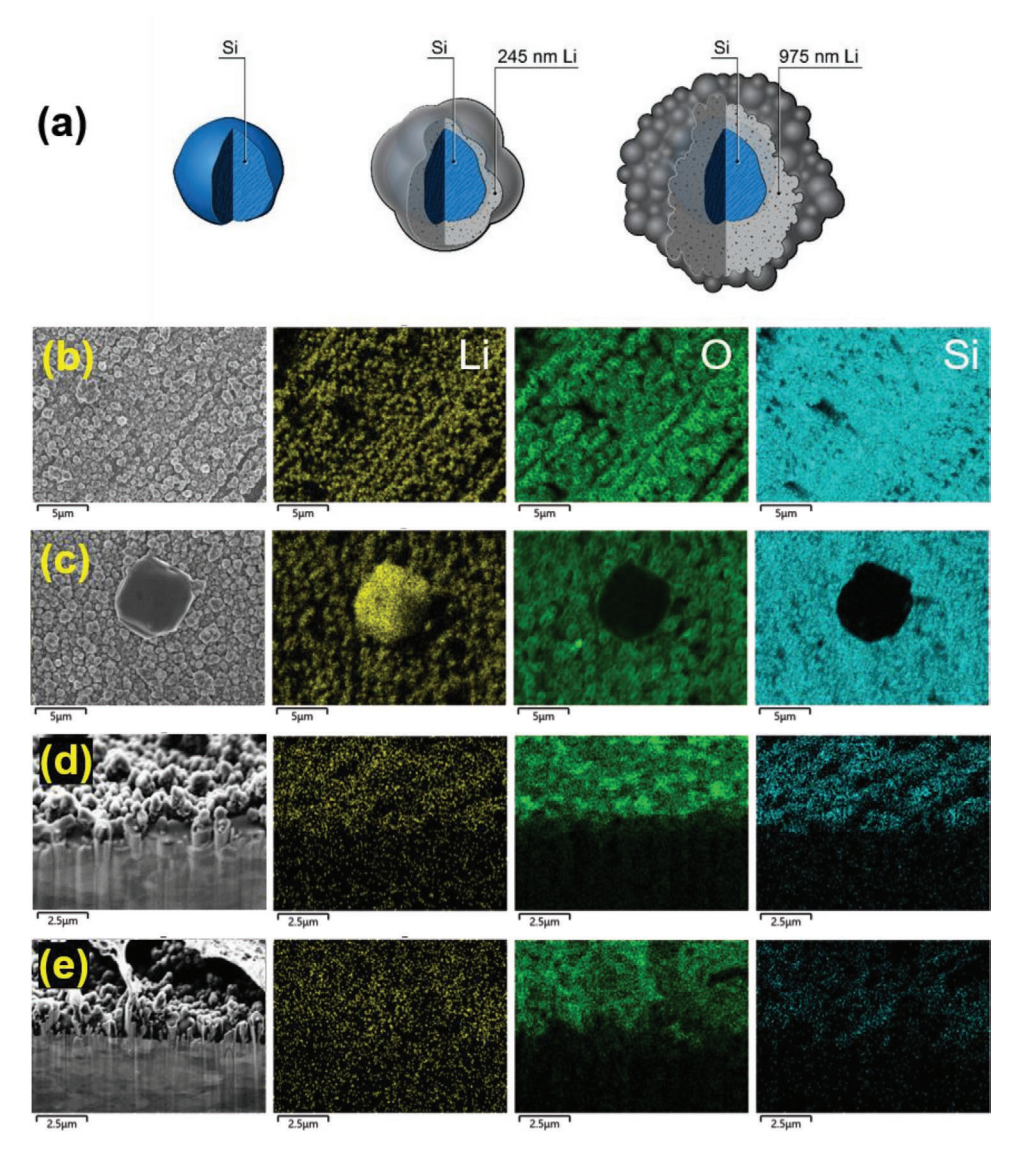


**Figure 1.** a) Schematic illustration of the deposited thin lithium metal on Si particle. Top view micrographs by SEM and elemental mapping by EDX of the b) Si + 245 nm Li, c) "Si + 975 nm Li" samples. Side view micrographs by cryo-FIB and elemental mapping by EDX of the d) Si + 245 nm Li, e) "Si + 975 nm Li" samples. The images were taken directly after Li deposition.

Experimental Section), the Li foil immediately melts and rapidly spreads across the electrodes. Two layers of Li with the thickness of 245 nm (further referred to as "Si + 245 nm Li") and 975 nm ("Si + 975 nm Li"), respectively, were deposited on top of Si thin film electrodes, as schematically depicted in **Figure 1a**. These values correspond to  $\approx\!40\%$  ("Si + 245 nm Li") and  $\approx\!100\%$  ("Si + 975 nm Li") pre-lithiation degrees which were confirmed by Li stripping of pre-lithiated Cu foil as well as the de-lithiation profiles of pre-lithiated Si as shown in Figure S2a,b, Supporting Information. It is important to note that once the Li is deposited on the Si surface, it reacts to create a binary lithium-silicide (Li\_xSi\_y) intermetallic phase. [17c,24]

Highly uniform Li deposition was successfully achieved as confirmed by top-view images by using scanning electron microscopy (SEM) combined with energy-dispersive X-ray spectroscopy (EDX) analysis for the elements Li, O, and Si, as shown

in Figure 1b,c. To check the homogenous in-depth Li distribution within the electrode, cryo-focused-ion beam (FIB) analysis was performed at the temperature of -150 °C to avoid sample damage. The corresponding cross-sectional EDX images for the different samples are shown in Figure 1d,e. As can be seen, Li is evenly distributed within the electrode regardless of the degree of pre-lithiation, proving that the Li on the interface was successfully infiltrated to the Si pores. Noteworthy, as Li is a lightweight element, the Li EDX-signal might overlap with those of other heavier elements. Therefore, although the Li-enriched area evidenced by EDX analysis shown in Figure 1b-e can give a general idea about the Li distribution, conclusions about Li quantification must be interpreted with caution. In this case, the "Si + 975 nm Li" sample shall appear more abundant and brighter compared to the "Si + 245 nm Li" sample. The EDX mapping also shows that the pre-lithiated electrodes contain

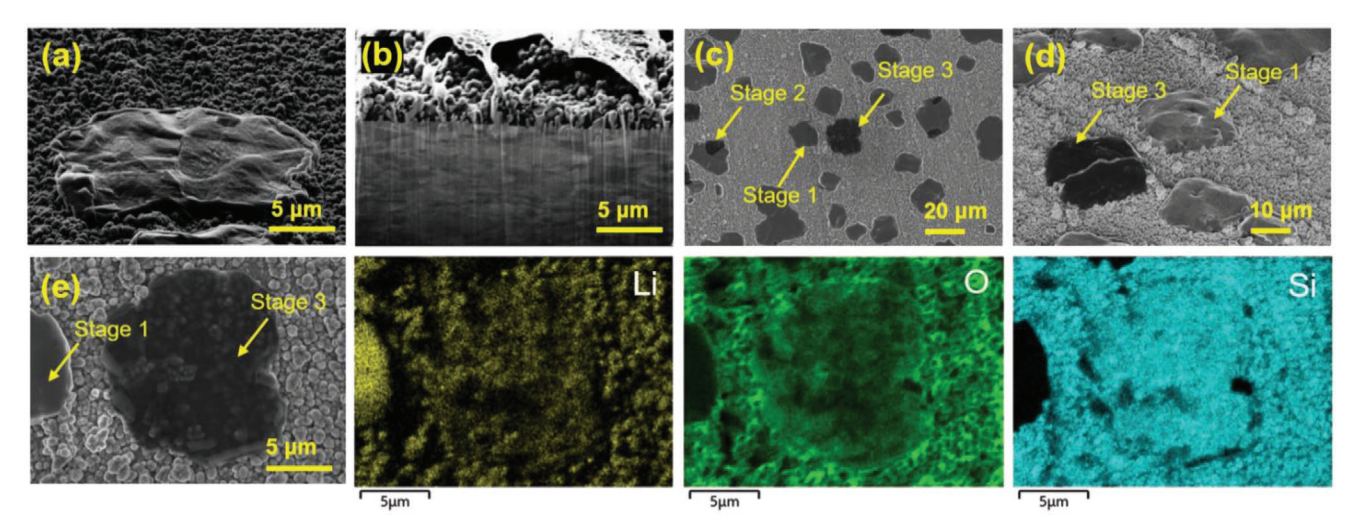


Figure 2. a) SEM image of pre-lithiated "Si + 975 nm Li" electrode (the sample was tilted 54°). b) Cryo-FIB image in the Li nucleation area of pre-lithiated "Si + 975 nm Li" electrode. SEM micrographs giving evidence of the slow alloying process in the dry-state pre-lithiation detected for the "Si + 975 nm Li" electrode: c) top-view, and d) tilted 54°. e) Observation of stage 3 by SEM and elemental mapping by EDX in the "Si + 975 nm Li" electrode.

rich concentrations of oxygen, suggesting the presence of a native layer of  $\text{Li}_2\text{O}$ . This was attributed to the spontaneously formed thin oxide layer under glove box or dry room atmospheres at the Li metal–air interface. Generally, after Li deposition on top of Si, the apparent morphology of Si particles is less spherical in comparison to the pristine Si thin film as shown from SEM images in Figure S3a–d, Supporting Information. Interestingly, the lower magnification SEM images revealed the presence of Li metal islands in the "Si + 975 nm Li" electrodes (Figure 1c; Figure S3d, Supporting Information (right)). In the classical theory, such Li metal islands can be ascribed to the Li nucleation where it is a new solid-phase associated with energy barrier related to the thermodynamic costs of forming the island cluster. [25]

During Li deposition, it is believed that the nucleation of a single Li atom on the Si surface occurs at first. As the number of Li atoms increases to a thick 975 nm, the electrochemical potential drops to ≈0 V at which is sufficient to drive the nucleation of Li. This condition allows the newly deposited Li atom on the surface to meet another Li atom without having interaction with Si particle and subsequently, these atoms join together to form a Li metal island (Figure 2a). This Li metal island covers the surface of the "Si + 975 nm Li" electrode with void space in between as revealed by the cryo FIB image shown in Figure 2b. In more detail, Figure S4a,b, Supporting Information shows a side-view comparison between the area where the Li metal island takes place and the area without the Li metal island. The sample was further stored in the dry-state (condition without electrolyte addition) for 2 weeks before being measured with SEM and EDX as shown in Figure 2c–e to observe its behavior. It seems clear that the Li nucleation phenomena in the drystate might experience three distinct observable stages: i) First, the formation of Li islands, followed by ii) the slow reaction of the Li islands with Si by an alloying lithiation mechanism, and finally iii) the complete reaction of deposited Li with the Si as indicated in Figure 2e where O and Si are present.

Figure S5, Supporting Information shows low magnification SEM images (for a fairer comparison) between the

"Si + 975 nm Li" electrodes which were measured immediately after Li metal deposition (Figure S5a,b, Supporting Information), and with the "Si + 975 nm Li" electrodes which were measured after 2 weeks storage time in the dry-state (Figure S5c,d, Supporting Information). As can be seen, there are no significant changes in Li metal island size for both samples, with an estimated size of  $\approx\!10\!-\!20~\mu\mathrm{m}$ . The relatively similar size may be due to the same thermodynamic energy needed to form the island clusters across the surface of the electrodes, as Si thin films have flat and homogeneous surfaces. The size of the Li metal island remains the same within 2 weeks due to slow reaction to the Si beneath.

Raman spectroscopy which mostly focuses on the lateral resolution was used to characterize the homogeneity of the pre-lithiated Si electrodes which were measured right after Li deposition. Results give evidence that Si thin film is uniformly lithiated as shown in optical images in Figure S6a-c, Supporting Information. The observable disappearance of the band associated with the a-Si peak at 480 cm<sup>-1[26]</sup> and the transition to the Li<sub>x</sub>Si<sub>y</sub> phase at 400 cm<sup>-1</sup> further confirms the lithiation of Si (Figure S6d,e, Supporting Information). This observation is in accordance with previous Raman measurements on the LixSiv phase.[27] Furthermore, a peak at 1853 cm<sup>-1</sup> can be noticed that might be attributed to the sample exposure to the laser during Raman measurement and trigger the formation of Li<sub>2</sub>C<sub>2</sub> as the Li could be melted. Another possibility is due to the decomposition of the Li<sub>2</sub>CO<sub>3</sub> formed on the Li surface since the vapordeposited Li is very reactive and the glove box is not 100% filled with Ar. Therefore CO<sub>2</sub> reacts with Li forming Li<sub>2</sub>CO<sub>3</sub> and thus transforms to Li<sub>2</sub>C<sub>2</sub>.<sup>[28]</sup>

The pre-lithiated Si electrodes were then further examined via X-ray photoelectron spectroscopy (XPS) with an Ar<sup>+</sup> sputter depth profiling to provide an overview of the lithiation depth (**Figure 3a**,b). The top surface of both electrodes was covered by a thin layer of Li which will serve as Li metal anode during electrochemical operation. After 3 min of Ar<sup>+</sup> sputtering in the "Si + 245 nm Li" electrode, three peaks in the core Si 2p spectra attributed to the Li<sub>x</sub>SiO<sub>y</sub> ( $\approx$ 101 eV), Si<sub>x</sub>O<sub>y</sub> (103 eV), and

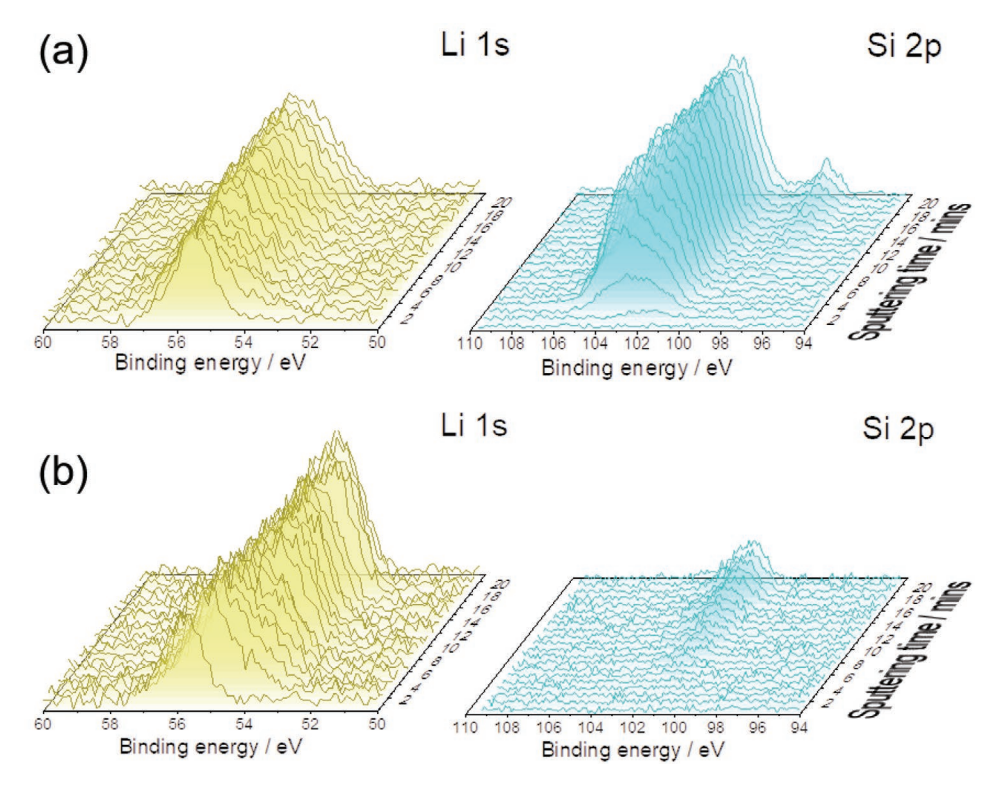


Figure 3. Li 1s and Si 2p depth profiling XPS core spectra of a) "Si + 245 nm Li" and b) "Si + 975 nm Li" electrodes in dry-state. The measurements were conducted immediately after Li deposition. Two independent samples for each material with three different positions were conducted.

SiO<sub>x</sub> (104 eV) become noticeable (Figure 3a; Figure S7a, Supporting Information, (top)).[29] This is the region where the top surface of Si underneath Li is reached. The formation of  $\text{Li}_x \text{SiO}_v$  originates from  $\text{Si}_x \text{O}_v$  or SiOH native oxide layer on Si thin films involved in the solid-state reaction with metallic Li. In the deeper regions, the highly reactive Li metal reacts with Si particles forming a Li<sub>x</sub>Si<sub>y</sub> alloy, as observed at binding energies of ≈98 eV (Figure S7a, Supporting Information (bottom)). The reaction then propagates throughout the surface of the film. Meanwhile, in the "Si + 975 nm Li" electrodes, the corresponding peak of  $\text{Li}_x \text{SiO}_v$  in Si 2p is visible only after 12 min of Ar<sup>+</sup> sputtering (Figure 3b; Figure S7b, Supporting Information (top)). The absence of a Li<sub>x</sub>Si<sub>y</sub> alloy peak even after further sputtering time confirms a thicker Li layer of this sample (see Figure S7b, Supporting Information (bottom)) in agreement with previous EDX results shown in Figure 1b,c.

# 2.2. Mechanism for Wet-State Pre-Lithiation of Si Electrodes: Addition of Electrolyte

The term "wet-state" represents the condition at which prelithiated electrodes are exposed to the organic carbonate-based liquid electrolyte (1 M LiPF<sub>6</sub> in ethylene carbonate (EC):ethyl methyl carbonate (EMC) (3:7 by wt) with 10 wt% fluoroethylene carbonate (FEC)). After Li deposition by PVD, the addition of electrolyte to the pre-lithiated electrodes makes the pre-lithiation mechanism much more complex, that is: 1) it induces pre-SEI formation by electrolyte decomposition since the potential of the electrode is lower than 0.4 V versus Li|Li<sup>+</sup>, hence, the

electrolyte is reduced, 2) faster pre-lithiation of the active material as the electrolyte provides a path for Li<sup>+</sup> ion movements, and 3) pre-volume expansion due to the faster alloying process. All these reactions occur simultaneously and immediately after the addition of the electrolyte.

#### 2.2.1. Alloying Reactions

The pre-lithiated Si in the wet-state was first examined by X-ray diffraction (XRD) analysis. For better comparison, the XRD pattern in the dry-state is also provided here. A very distinct pattern was detected from the samples in the dry-state and wetstate (Figure 4a,b). In the dry-state, reflections are absent probably due to the amorphous character of the Si thin film and the slow/no Li-Si reaction (Figure 4a). In other words, only Li that is in contact with Si will react, while Li metal in the upper layer(s) has no path to react with Si. In Figure 4b, the reflections which appear after electrolyte addition are an indication of the Li-Si alloying reactions. Main reflections found in "Si + 245 nm Li" electrodes could be attributed to the formation of Li<sub>12</sub>Si<sub>7</sub>, Li<sub>13</sub>Si<sub>4</sub>, and Li<sub>15</sub>Si<sub>4</sub>.<sup>[30]</sup> Further, a rather increased intensity of crystalline Li<sub>15</sub>Si<sub>4</sub> reflections was found for the "Si + 975 nm Li" electrode compared to the "Si + 245 nm Li" electrode, giving evidence of a deeper lithiation state of Si, in good agreement with previous works. [31] Accordingly, the slight discrepancy reflections appearance between "Si + 245 nm Li" and "Si + 975 nm Li" could also be attributed to the thickness of the samples that may be too thin to satisfy Bragg's law. In this case, some reflections may have been missing.

www.afm-journal.de

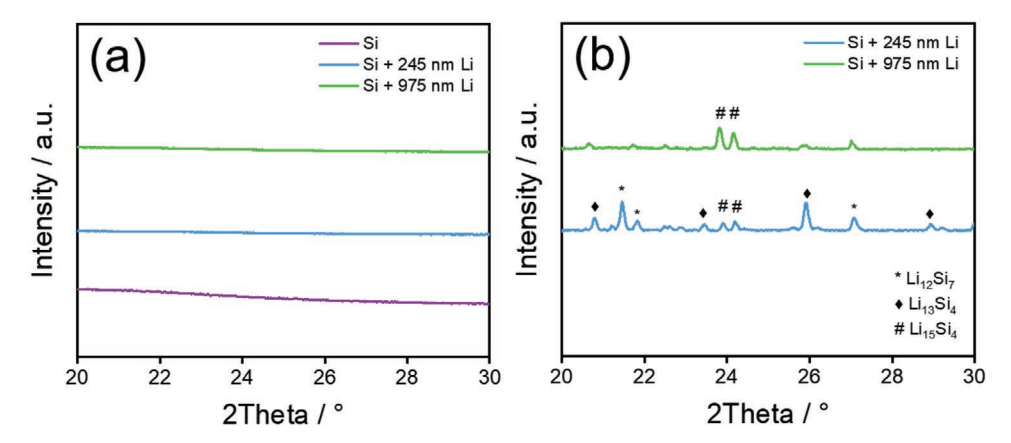


Figure 4. Pre-lithiation effect on Si thin film negative electrodes. XRD patterns of various electrodes a) in dry-state (immediate measurement) and b) in wet-state 48 h after electrolyte addition. The reflections in the dry-state are independent of the time since similar reflections can be seen even when the samples are stored for 2 weeeks. In the wet-state, the choice of 48 h prior to the measurement is to let the samples experience Li-Si alloying reaction (48 h means the samples have entered region III which will be explained later as depicted in Figure 5b).

#### 2.2.2. Consumption of Excess Li Metal

Adv. Funct. Mater. 2022, 32, 2201455

OCV profiles of the samples in wet-state conditions were recorded for 6 h after cell assembly to observe the lithiation behavior of the electrodes (Figure 5a). In the resting time of 6 h, two different phenomena were observed. The "Si + 245 nm Li" sample exhibits an OCV of ≈0.4 V and experiences a sudden voltage increase, while the "Si + 975 nm Li" electrode has an OCV of ≈0 V and experiences a sudden voltage drop. The obvious difference in OCV for both samples is due to different Li amounts which lead to a different degree of pre-lithiation.

In the "Si + 245 nm Li" sample (≈40% pre-lithiation degree), Li is less likely to cover the whole Si surface due to the lower degree of available Li for pre-lithiation, meaning there might be local spots where Li metal is present and there are locations where it is not (as schematically illustrated in Figure 5c). Thus, the electrodes will experience many differences in utilization of the Si particles (spots with remaining bulk Li metal will be different from spots without Li metal) causing locally different electrode potentials leading to an overall mixed electrode potential, cf. explanations in refs. [32] The voltage increase as shown in Figure 5a for "Si + 245 nm Li" suggests that

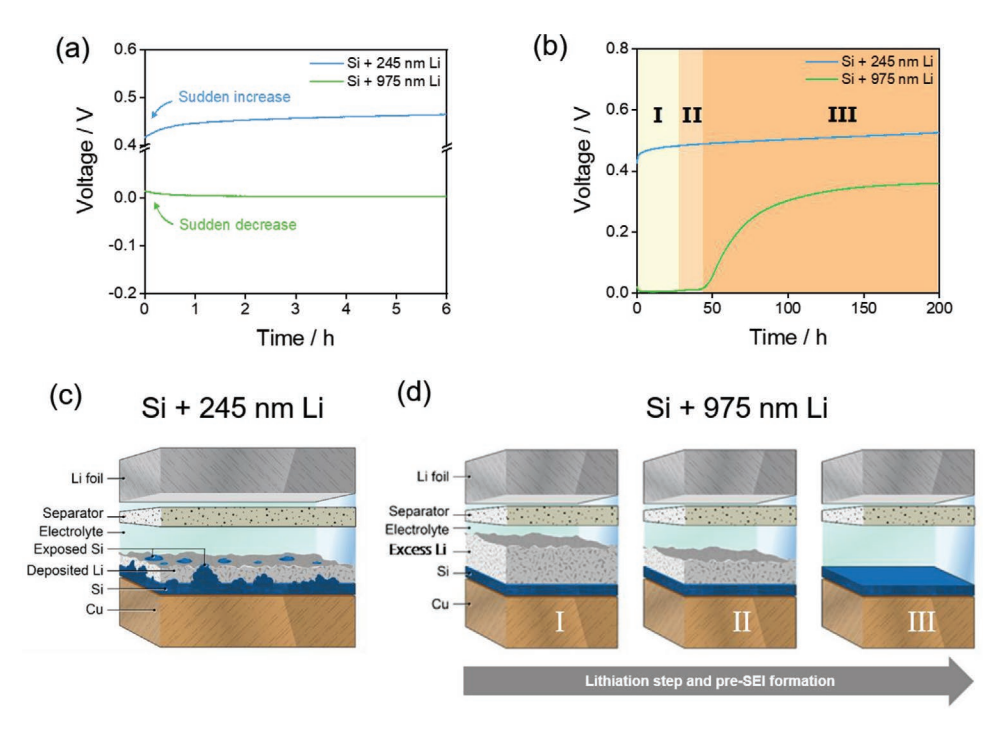


Figure 5. OCV development of SillLi metal cells using "Si + 245 nm Li" and "Si + 975 nm Li" electrodes with a) 6 and b) 200 h resting time after addition of the electrolyte (1 M LiPF<sub>6</sub> in EC:EMC 3:7 by wt + 10 wt% FEC). c) Schematic illustration of wet-state pre-lithiation of the "Si + 245 nm Li" electrodes, d) schematic illustration of Li consumption by lithiation and pre-SEI formation in the wet-state "Si + 975 nm Li" electrodes.

ADVANCED FUNCTIONAL MATERIALS

self-discharge is taking place. [20] Considering that Si and Li metal may be present, self-discharge involves Li metal dissolution at low cell voltages and de-lithiation of  $\text{Li}_x \text{Si}_y$  at higher voltages. Another aspect that may contribute to voltage changes is the competition of Li consumption between two mechanisms, that is, 1) pre-lithiation of the active Si material (with the simultaneous dissolution of Li metal) and 2) consumption of Li for pre-SEI formation.

Meanwhile, in the "Si + 975 nm Li" sample, the OCV up to 6 h is  $\approx 0$  V which indicates Li metal as one electrode is as if being paired with Li metal film (on Si) as the other electrode, implying vapor-deposited Li was covering the whole Si surface and confined within the porous substrate surface (dendritic Cu + Si). The excess Li on the Si surface will not allow the electrolyte to penetrate to the Si thin film beneath for some time. There is no driving force for the Li to react despite being exposed to the electrolyte. Only the Li that is in contact with Si will experience alloying reaction to form the c-Li<sub>15</sub>Si<sub>4</sub> phase as found in previous work. [17c] The excess Li metal on the Si surface keeps the potential of the Si electrode nearly the same as the potential of pure Li metal.

The OCV profile was then held for 200 h for both electrodes as can be seen in Figure 5b. The "Si + 975 nm Li" shows a clear voltage increase that can be divided into three regions: region I, region II, and region III, respectively. In the first 28 h (corresponding to region I), the potential of the electrode does not change which means the electrolyte is unable to penetrate to the deeper region and is only in contact with excess Li metal. The voltage starts to increase in region II (28-47 h) which explains a small part of excess Li is used up for pre-SEI formation. In region III, the curve increases exponentially to 0.36 V (47-150 h) followed by a nearly steady voltage plateau up to 200 h. We believe at this point the excess Li is completely consumed as a consequence of pre-SEI formation, Li metal dissolution at low voltages, and de-lithiation of Li, Si, at higher voltages. To the best of our knowledge, this is the first report to establish in situ pre-SEI formations via lithium evaporation and subsequent electrolyte addition before cell operation. Thus, due to the presence of the pre-SEI formation, Li<sup>+</sup> from the cathode will not be consumed and the pre-lithiated Si electrodes will have minimum capacity (=active lithium) loss. Therefore, it is expected that the cell will have an improved capacity retention. The schematic, showing the transformations from region I to region II and eventually to region III in the "Si + 975 nm Li" sample, is described schematically in Figure 5d.

The first charge/discharge cycle of the pre-lithiated electrodes was analyzed at 0.1 C in Si||Li metal cells. Figure S8a, Supporting Information shows lithiation/de-lithiation capacities of pristine Si, "Si + 245 nm Li," and "Si + 975 nm Li" with 6 h resting time, respectively. A common nominal lithiation capacity was obtained for pristine Si. The lithiation capacities for "Si + 245 nm Li" and "Si + 975 nm Li" electrodes were  $\approx 2000$  and  $\approx 0$  mAh g $^{-1}$ , respectively. When the resting time was increased to 200 h, the specific lithiation capacity for both pre-lithiated Si electrodes increased to  $\approx 2470$  mAh g $^{-1}$  for "Si + 245 nm Li" and  $\approx 290$  mAh g $^{-1}$  for "Si + 975 nm Li," respectively (Figure S8b, Supporting Information). The change of capacity as a function of resting time is most likely attributed to the consumption of excess Li.

# 2.2.3. Phase Transformations of Pre-Lithiated Si During (De-)lithiation

The other unique behavior is the increase in de-lithiation capacity which has been never seen in other pre-lithiation techniques (Figure S8c,d, Supporting Information). With 6 h resting time Si, "Si + 245 nm Li," and "Si + 975 nm Li" electrodes can reach de-lithiation capacities of 2770, 2960, and 3750 mAh g<sup>-1</sup>, respectively. The pre-lithiated Si electrodes might experience homogeneous crystallization which typically involves preceding nucleation from a single phase and its subsequent grain growth. [33] In other words, a two-step mechanism applies as proposed by Jiang et al., where there is an electrochemical step that forms critical nuclei of Li<sub>15 +  $\delta$ </sub>Si<sub>4</sub> ( $\delta$  represents a very small increment of lithium) from single phase followed by the growth of the nuclei to the c-Li<sub>15</sub>Si<sub>4</sub> phase. [34] This would explain the slight de-lithiation capacity increase as the degree of pre-lithiation increases.

Clear differences between samples can be seen from the first cycle voltage profile and the differential capacity (dQ/dV)versus voltage plots as depicted in Figure 6a-c. The pristine Si and "Si + 245 nm Li" show similar voltage curves except in region I. The lithiation of pristine a-Si shows a rather sloping potential profile as typical for a single-phase reaction indicating Li<sup>+</sup> ions enter a Si-dominated environment (Figure 6a,c; I). For the case of "Si + 245 nm Li," the environment is already dominated by  $\text{Li}_x \text{Si}_v$  from the beginning. This is the reason why the first cathodic peak of "Si + 245 nm Li" exists with lower intensity compared to the pristine a-Si (Figure 6c; I). As the cut-off voltage does not go below a limit of 50 mV, the Si maintains its amorphous character and forms the final amorphous product a-Li<sub>x</sub>Si<sub>y</sub> for both electrodes (region II).<sup>[35]</sup> The subsequent process indicated by regions III and IV corresponds to the delithiation of a-Li, Si,.

The "Si + 975 nm Li" electrodes show a distinct voltage profile. The flat plateau (Figure 6b; V) and the second anodic peak (Figure 6c; V) correspond to the stripping process of excess Li metal that remained on Si thin films after 6 h resting time and the amount can be estimated based on the length of the stripping voltage plateau. Since the voltage is  $\approx$ 7.4 mV which lies within the voltage range where the c-Li<sub>15</sub>Si<sub>4</sub> phase forms (<50 mV), thus one single intense peak at  $\approx$ 0.45 V from the dQ/dV plot is detected during de-lithiation (Figure 6c; VI) and a single-wide plateau substantiates the coexistence of two-phase region (Figure 6b; VI). Since the voltage is  $\approx$ 7.4 mV

The reaction of Si with Li in the regions I–VI can be summarized as follows:

I and II :  $y(a-Si) + xLi^+ + xe^- \rightarrow a-Li_xSi_y$ III and IV :  $a-Li_xSi_y \rightarrow y(a-Si) + xLi^+ + xe^-$ 

V : Li metal stripping

 $VI : c-Li_{15}Si_4 \rightarrow 4a-Si + 15Li^+ + 15e^-$ 

The crystallization behavior is further discussed in detail from the results of constant current charge/discharge using different resting times shown in Figure S9a,b, Supporting Information. The first sample is pristine Si when discharged with a constant current of 0.1C to 7.4 mV (same as the OCV of "Si + 975 nm Li"). The second sample is "Si + 975 nm Li" with a 6 h resting time, and the third sample is "Si + 975 nm Li" with 200 h resting time. In alignment with reported literature, when

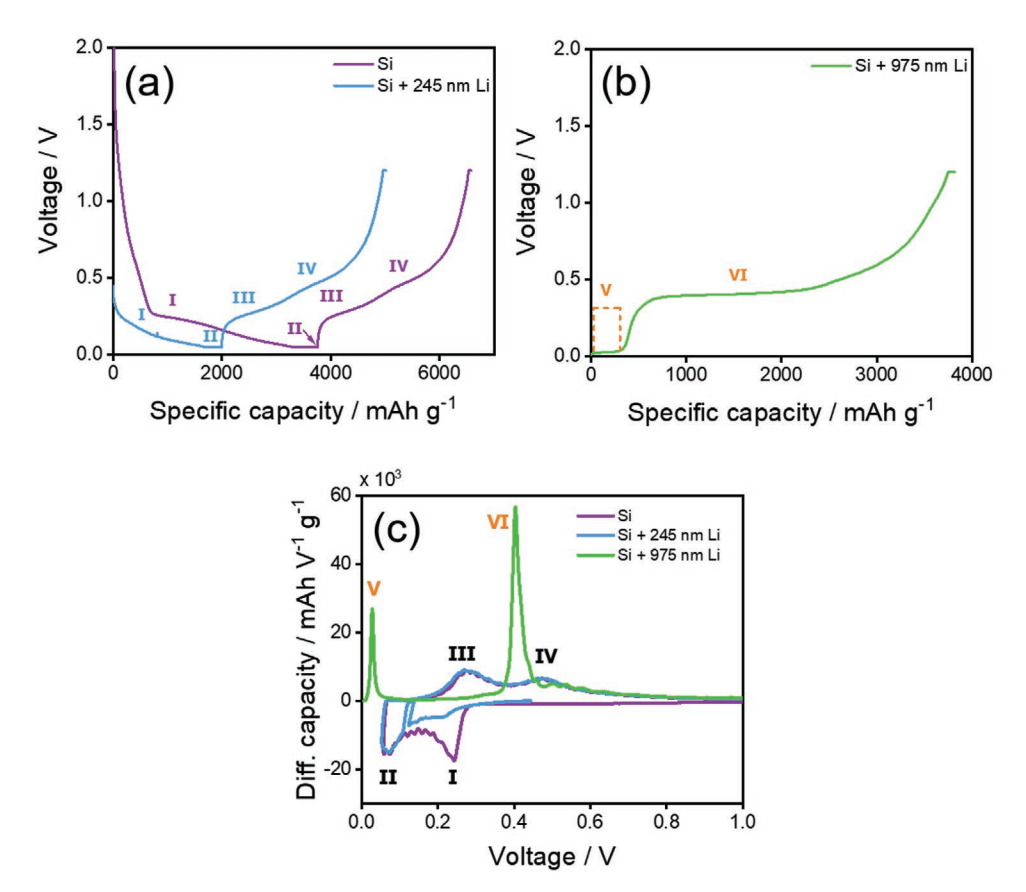


Figure 6. Electrochemical characterization of different Si||Li metal cells: a,b) 1st cycle voltage profile at 0.1 C, and c) corresponding differential capacity (dQ/dV) versus voltage plots of the 1st cycle. The pristine Si was discharged until reached 50 mV. All cells were rested for 6 h prior to the cell operation.

the voltage of Si falls below 50 mV, the reaction is associated with an abrupt formation of crystalline Li $_{15}$ Si $_4$  as characterized from an intense peak at  $\approx$ 0.45 V in the dQ/dV plot (Figure S9b, Supporting Information). [35a,38] For the "Si + 975 nm Li" electrodes, regardless of resting time, the existence of c-Li $_{15}$ Si $_4$  is confirmed which suggests that the a-Li $_x$ Si $_y$  rapidly crystallized. This phenomenon can be considered equivalent to the delayed freezing of super-cooled water below 0 °C, in which liquid water can remain totally free of ice for a certain period before the transition to ice. From the figure, one also can conclude that there is no Li stripping process in the "Si + 975 nm Li" electrodes after being rested for 200 h suggesting no remaining excess Li.

## 2.3. Surface Analyses of Pre-Lithiated Si Electrodes in Dry-State versus Wet-State

Figure S10a,b, Supporting Information shows the morphological and structural differences of the "Si + 245 nm Li" and "Si + 975 nm Li" in the dry-state and wet-state (before and 48 h after electrolyte addition). In the dry-state, Li metal is visible on the outer surface of Si for both samples ("Si + 245 nm Li," and "Si + 975 nm Li"), without the presence of any cracks in the surface. In the wet-state, the observed morphological behavior is in strong contrast to that observed in the dry-state, revealing the formation of several cracks due to lithiation of Si as well as the

associated volume change. The former gaps between the Si particles have also diminished which might be caused by the accumulation of SEI decomposition products due to the reaction between  $\text{Li}_x \text{Si}_y$  with the added electrolyte. This chemomechanical appearance of the  $\text{Li}_x \text{Si}_y$  phase has been expected, and it is analogous to that of electrochemically lithiated Si anodes. [39]

Another striking observation is shown in Figure 7a-d. Surface morphologies of pristine Si and "Si + 975 nm Li" (drystate) are shown in Figure 7a,b, respectively. The comparison of fully electrochemically lithiated pristine Si and wet-state "Si + 975 nm Li" electrodes is also provided in Figure 7c,d, respectively. This is a fair comparison as both electrodes experience a similar voltage (~7.4 mV). Large cracks and expanded surfaces are observed for the electrochemically lithiated pristine Si electrodes (Figure 7c). The obvious cracks in the micrometer range suggest that the large volume change occurred in electrochemically lithiated Si causing the disconnection of the active material particle and inducing large Li losses. In the worst case, if the active materials are detached, the electronic connection to the substrate that is necessary for the electron transfer would be lost, too.<sup>[40]</sup> Contrarily, SEM images reveal excellent integrity with rather moderate cracks across the surface of the wet-state "Si + 975 nm Li" electrode (Figure 7d). This moderate crack is a consequence of the pre-SEI formation. Electrodes maintain the original morphology despite the occurrence of the alloying process. The robust connections tightly hold the Si particles together to resist the disconnection of active materials.

www.afm-journal.de



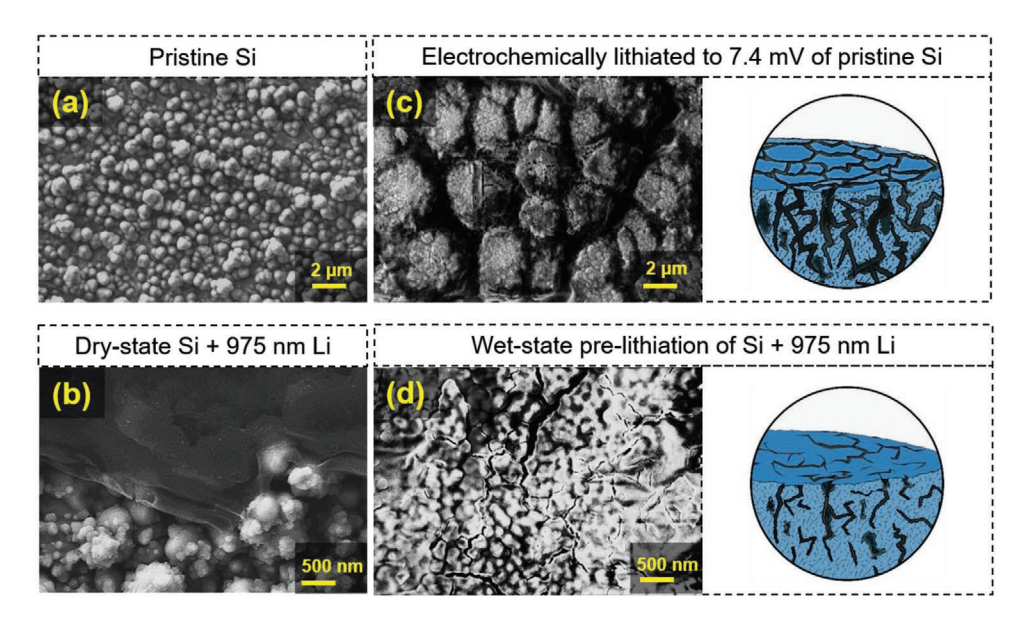


Figure 7. Visualizing of surface crack and volume expansion. SEM micrographs of a) pristine Si before electrochemical lithiation, b) dry-state "Si + 975 nm Li," c) electrochemically lithiated pristine Si to ≈7.4 mV at 0.1 C, and d) wet-state pre-lithiation of "Si + 975 nm Li." In the wet-state, the measurements were conducted 48 h after electrolyte addition.

Therefore, thermal evaporation of Li is a highly promising option for the pre-lithiation of Si-based anodes which provides not only a precise pre-lithiation degree but also induces a pre-SEI formation for better utilization and stabilization of highvolume-change electrode materials and avoids continuous Li losses in practical LIB cells.

#### 2.4. Electrochemical Reversibility in SillLi Metal Cells

The initial five cycles of cyclic voltammetry (CV) plots of the three electrodes are compared to study the reversibility of the lithiation/de-lithiation processes, as well as the Li+ ion transport properties under the influence of pre-lithiation as shown in Figure S11a-c, Supporting Information. For the case of pristine Si as shown in Figure S11a, Supporting Information, the occurrence of only one cathodic peak at ≈0.05 V in the first and second cycle is due to the fact that the scan rate (25  $\mu$ V s<sup>-1</sup>) is most likely too fast to fully lithiate the pristine Si thin film (here the thickness is 300 nm) in these two cycles. From a previous publication,<sup>[41]</sup> a clear cathodic peak at ≈0.3 V could be observed for Si thin film with a lower thickness (140 nm) using the same scan rate, which supports the assumption of the too fast scan rate considering a more than double electrode thickness in our work. In the third and further scans, the Si has expanded and more area for the electrode|electrolyte interface has been created allowing to fully lithiate the Si even at the applied fast scan rates. Thus, in the 3rd-5th cycle, the current peaks show better (de-)lithiation reversibility. Figure S11b, Supporting Information shows that the lithiation of "Si + 245 nm Li" starts from ≈0.4 V. In the first cycle, the presence of one cathodic peak at 0.05 V implies that the Li directly enters a Li<sub>x</sub>Si<sub>v</sub> dominated environment.<sup>[35]</sup> During the anodic scan, the peaks located at ≈0.3 and ≈0.5 V evidence the discharge reaction of Li (vapordeposited Li and the Li inserted in Si) transforming the LixSiv

phases to a-Si.[42] In Figure S11c, Supporting Information (showing "Si + 975 nm Li"), no cathodic peaks are found in the first cycle as the electrolyte cannot penetrate to the active material since excess Li covers the Si surface, thus no lithiation reaction of Si occurs. Similar to the dQ/dV versus voltage profile, the anodic peak at ≈0.1 V in the CV experiment is due to Li stripping and another peak at ≈0.45 V is the characteristic de-lithiation peak of c-Li<sub>15</sub>Si<sub>4</sub>. In the subsequent cycles, highly reversible CV curves without obvious changes were observed, suggesting that the Si has been "activated," revealing improved (de-)lithiation reversibility.

To further investigate the beneficial impact of pre-lithiation by means of vapor-deposited Li and resting time on the longterm material stability, room-temperature constant current charge/discharge cycling of SillLi metal cells was performed at a rate of 0.5C for 200 cycles (Figure 8a,b). Figure 8a shows the specific capacity as a function of cycle number and Figure 8b shows the normalized specific capacity (100% was considered from the first discharge capacity at 0.5C). Due to the formation of a large Li reservoir and pre-SEI formation, "Si + 975 nm Li" shows the most stable and the highest capacity retention, followed by "Si + 245 nm Li" regardless of the resting time. In contrast, pristine Si shows significant capacity fading, possibly due to the extensive SEI accumulation and volume changes during cycling. Nonetheless, it is difficult to comment on differences in Coulombic efficiency ( $C_{Eff}$ ) since the values of the individual electrodes are close to each other.

Thus, to have a better understanding of  $C_{Eff}$  evolution, the accumulated Coulombic inefficiency (ACI<sup>[43]</sup>) and accumulated irreversible capacity (AIC[43]) are provided in Figure 8c,d and Figure S12a,b, Supporting Information comparing the pre-lithiated electrodes with pristine Si. The "Si + 975 nm Li" electrodes with 6 h resting time surprisingly show higher ACI and AIC compared to "Si + 245 nm Li" and even pristine Si. This phenomenon suggests that there might be a sweet spot

www.afm-journal.de

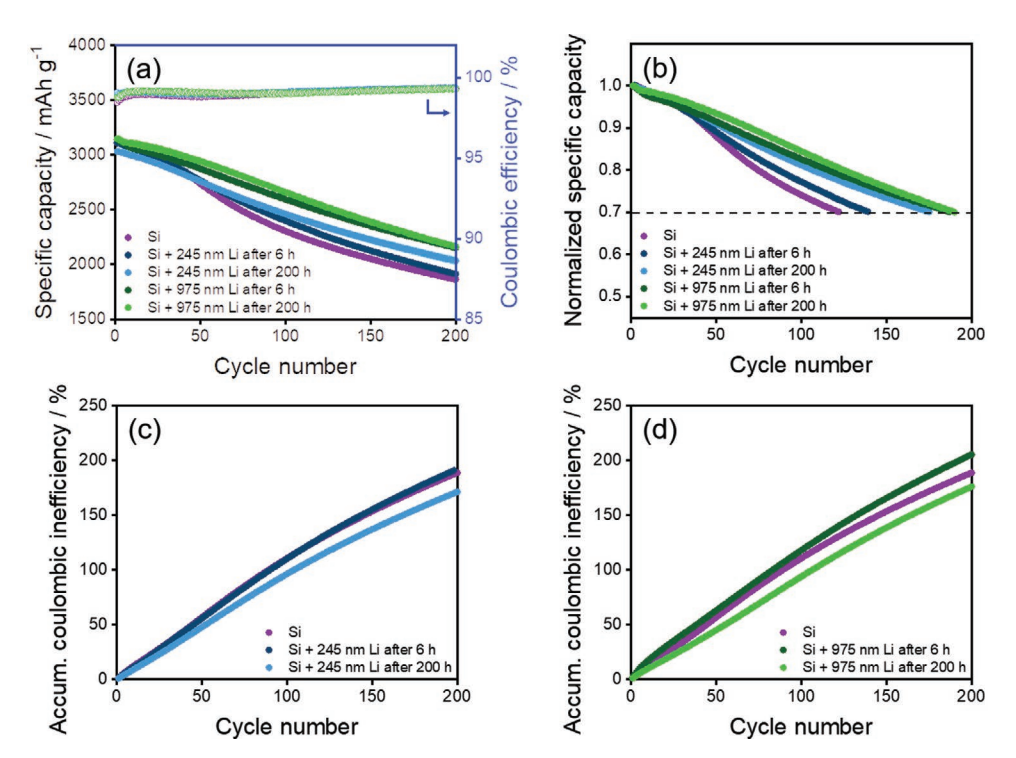


Figure 8. Electrochemical evaluation of various Si||Li| metal cells after different resting times at 0.5 C. Specific capacities as a function of a) cycle number, and b) normalized specific capacity up to 70% state-of-charge (100% was considered from the first discharge capacity at 0.5 C). Accumulated Coulombic inefficiencies for c) "Si + 245 nm Li," and d) "Si + 975 nm Li" using different resting times. The pristine Si profile is added as a baseline. Errors represent the standard deviation of three cells per type of sample to ensure reproducibility.

between the thickness of Li metal and the thickness of Si thin films, which impacts the degree of pre-lithiation and electrochemical performance. However, we believe, higher ACI and AIC of the "Si + 975 nm Li" electrodes are compensated and not taken into the consideration to affect the stability and capacity retention performance. With the usage of 200 h resting time followed by three formation cycles at 0.1 C, the excess Li metal on the surface was completely removed and promoted remarkably lower ACI and AIC for "Si + 975 nm Li" and eventually suppressing active Li loss (Figure 8d; Figure S12b, Supporting Information). This behavior also can be seen for "Si + 245 nm Li" electrodes (Figure 8c; Figure S12a, Supporting Information). Thus, we conclude that the parasitic reactions, which increase the AIC and ACI due to electrolyte decomposition, seem to be significantly reduced after long resting times (200 h) for prelithiated Si.

To give further insights into differences in the electrochemical data shown above, Figure S13a–c, Supporting Information shows the lithiation/de-lithiation capacities at the first cycle using different resting times. For comparison, the data of the pristine Si electrode is also plotted. With 6 h resting time, the irreversible capacity of "Si + 975 nm Li" is 80 mAh g $^{-1}$ , which is higher than the case of the "Si + 245 nm Li" (44 mAh g $^{-1}$ ) or even that of the pristine electrode (49 mAh g $^{-1}$ ). However, after 200 h resting time, the irreversible capacity of "Si + 975 nm Li" decreases significantly to 30 mAh g $^{-1}$  (62% lower), while for "Si + 245 nm Li" decreases to 29 mAh g $^{-1}$  (34% lower). This is further proof that an appropriate resting time is needed when the electrodes are pre-lithiated to reduce parasitic reactions.

With ongoing cycling, the same pattern was observed as shown from Figure S14a–c, Supporting Information. Thus, pre-lithiation with a thermal evaporation technique is an effective way to create effective SEI formation and proper resting times are necessary to avoid undesirable reactions because of excess Li metal.

Overall, the proposed Li thermal evaporation brings a novel concept to introduce a new technique with a great promise and will be of significant value to academic researchers and even to industrial applications. This work has revealed the importance of uniform Li distribution of pre-lithiation and demonstrated a novel method to achieve it. The uniform Li distribution induces pre-SEI formation, creates moderate surface cracks, and increases reversibility during cycling. Further works will focus on investigating the electrochemical performance of pre-lithiated Si anodes in realistic full-cells. In addition, although there would be a lot of challenges in achieving the desired degree of pre-lithiation, the application toward practical Si-based electrodes, such as silicon/graphite composite electrodes, will be the main focus of further research.

#### 3. Conclusion

In this work, pre-lithiation of Si thin films was conducted through thermal evaporation of Li metal to mitigate active lithium losses in Si-based cells. The proposed pre-lithiation techniques overcome the challenges of existing pre-lithiation techniques by using passivated Li metal powder or Li metal

ADVANCED FUNCTIONAL MATERIALS

foil, that is, the ability to precisely control the degree of prelithiation and to enable a highly homogeneous Li metal deposition at the anode surface. We showed that a highly uniform Li distribution compensates for the typical Li loss occurring during cycling. The results clearly show that if such measures are not taken into account, the particle-by-particle utilization/ lithiation differs and increase safety risks. We have discussed important parameters such as Li nucleation and pre-lithiation conditions (dry-state and wet-state, i.e., without and with liquid electrolyte). In the dry-state, the absence of crystalline phases indicated the relatively slow reaction (=lithiation) between Si and the vapor-deposited Li. In wet-state, the conditions are much more complex due to pre-SEI formation by electrolyte decomposition, Li dissolution at low voltage, de-lithiation of Li<sub>r</sub>Si<sub>v</sub> at higher voltage, and the competition of Li consumption. These phenomena are all taking place simultaneously and subsequently. Further, we comprehensively analyzed the impact of the pre-volume expansion and moderate mechanical crack formation on the electrochemical performance with respect to resting time. Finally, this work opens up a new approach and a further understanding of pre-lithiation studies for high-capacity Si anodes in LIB cells. The pre-SEI formation described here is therefore a promising strategy to achieve an even enhanced lifetime of high-energy LIB cells.

## 4. Experimental Section

Si Thin Film Electrode Preparation: Magnetron sputtering was used to deposit silicon as a negative electrode (purity 99.99%; resistance  $<0.02~\Omega;$  FST Freiberger Silicium and Targetbearbeitung GmbH) on a dendritic copper foil (Carl Schlenk) acting as a current collector, and the thickness was controlled by the deposition time (distance = 7 mm and base pressure =  $10^{-7}$  mbar). In the beginning, the chamber was flushed with argon and the plasma was ignited at a pressure of  $5\times10^{-2}$  mbar at an RF-power of 90 W. The substrate holder was continually rotated at a speed of 10 rpm to ensure homogeneous deposition. When the desired thickness was reached ( $\approx300~\mu\text{m}$ ), the system was brought back to initial conditions. The deposition thickness was determined by the deposition on a silicon wafers substrate (Siltronic) through a profilometer (Bruker Dektak XT). The weight of each Si thin film electrode (Ø12 mm;  $\approx65.55~\mu\text{g}~\text{cm}^{-2}$ ) was determined by sputtering 25 samples and averaging the weight.

Pre-Lithiation of Si Thin-Film Negative Electrodes by Thermal Evaporation: The thin layer Li was deposited by the PVD method on top of Si thin films using the ProVap PVD system (MBRAUN). The process was based on a resistive heating approach, where Li metal ingots were placed in an evaporation tantalum boat and a high electric current combined with a low voltage was applied to melt and vaporize the material. The maximum electric power delivered by the system was 2000 W and for Li metal, an average of 15% of the total power was used.

Deposition takes place at a high vacuum of about  $10^{-6}$  mbar in the ProVap PVD chamber integrated with a glove box (MBRAUN) filled with argon (Ar) at  $H_2O$  concentrations below 0.2 ppm and  $O_2$  levels < 0.1 ppm. To minimize contamination, the entire glove box was flushed several times with fresh Ar before each coating process. Also, the box and chamber were baked out several times with a heat gun at 200  $^{\circ}$ C.

The evaporation process was controlled by an SQC-310 controller (Inficon) using gold-coated quartz crystal sensors operating at 6 MHz. Here the final film thickness, deposition rate, and further heating parameters could be adjusted. The substrate was secured on the substrate holder facing down to the evaporation source and kept in rotation of 10 rpm. Also, the substrate was protected by a shutter until

the desired deposition rate of 5 Å s $^{-1}$  was reached. When the desired deposition rate was kept constant, the shutter opens and the substrate could be coated. Once the desired thickness was achieved, the samples were transferred to an air-tight sample holder to avoid air exposure. However, the deposited thin layer Li was highly reactive as it had no native protection layer. In this configuration, the formation of  $\text{Li}_2\text{O}$  was most likely to happen.

Electrochemical Investigation of Pre-Lithiated Si Electrodes: All electrochemical investigations were carried out in a-Si||Li metal cell (twoelectrode configuration [44]) in CR2032 coin cells (Hohsen Corporation) using Li metal foil (Albemarle; purity: battery grade) as a negative electrode. A Ø15 mm separator (Celgard 2500, polypropylene) was placed between the two electrodes. All cells were filled with 50 uL batterygrade (BASF) which contained 1 M lithium hexafluorophosphate (LiPF<sub>6</sub>) in EC/EMC (3:7 by weight) with 10 wt% FEC as SEI-forming additive. For electrochemical experiments, all cells had a rest period of 6 h at OCV unless stated otherwise. The cells were cycled in a voltage range of 0.05 to 1.2 V unless stated otherwise. Cells were cycled for three cycles at a charge/discharge rate of 0.1 C (1 C corresponds to 3500 mA g<sup>-1</sup>) and at 0.5 C for 200 cycles. After the lower voltage was reached, a constant voltage step was performed until reaching a specific current of  $\leq$ 0.05 C ( $\leq$ 175 mA g<sup>-1</sup>). All electrochemical measurements were carried out on a Maccor series 4000 battery tester at room temperature. For CV, measurements were carried out on a VMP multichannel constant voltage-constant current system (Bio-Logic Science Instruments) at room temperature. The same voltage range to galvanostatic charge/discharge was applied and the scan rate was 25  $\mu V$  s<sup>-1</sup>. All electrochemical studies were performed at least three times to ensure a sufficiently high reproducibility.

Characterization Methods: The morphology of the samples was characterized using a SEM (Carl Zeiss AURIGA; Carl Zeiss Microscopy GmbH). The SEM images were taken using a working distance between 3.5 and 4 mm and an accelerating voltage of 3 kV. EDX was measured with an Ultim Extreme detector to evaluate the elemental composition of the samples. The spectra were evaluated with the INCA software (Oxford Instruments). The cryo-FIB (Zeiss Ion sculptor FIB-column; Carl Zeiss Microscopy GmbH) was employed to cut the Li-containing electrode at -150~°C to avoid Li melting.

The crystallinity and phase changes of the pre-lithiated Si electrodes were analyzed by ex situ Raman spectroscopy and XRD. To record XRD patterns and to determine the phase transformation, a Bruker D8 Advance X-ray diffractometer (Bruker AXS GmbH) with a Cu-K $\alpha$  wavelength of 0.154 nm and with a divergence slit of 0.5° was used. Raman spectra of pre-lithiated Si electrodes were recorded with a Raman microscope (Bruker SENTERRA, Bruker Optics Inc.) operating at a wavelength of 532 nm and using 0.2 mW of excitation

XPS was performed to analyze the SEI formed on the pre-lithiated Si. The samples were transferred to the XPS device (Axis Ultra DLD, Kratos) with minimum exposure to ambient air in a sealed container. Monochromatic Al K $\alpha$  X-rays (h $\nu=$  1486.6 eV) with a 10 mA emission current and 12 kV accelerating voltage were applied. The pressure within the analysis chamber was  $10^{-9}$  mbar. The analysis area was  $\approx 100~\mu m^2$  with a sputter crater size of  $\approx 2~mm^2$ . A charge neutralizer was used to compensate for the charging of the samples. The measurement was performed at a 0° angle of emission and a pass energy of 20 eV. The data fitting was carried out with CasaXPS. Calibration of the EBinding was performed by using the C 1s C-H/CC peak ( $E_{\rm Binding}=284.8~{\rm eV}$ ) as an internal reference. Sputter depth profiling was carried out using Ar $^+$  as ion source (4 kV, 50  $\mu{\rm A}$  extractor current). For checking the reproducibility, three different measurement spots per sample were investigated.

#### **Supporting Information**

Supporting Information is available from the Wiley Online Library or from the author.

www.afm-iournal.de

#### ADVANCED FUNCTIONAL MATERIALS

### Acknowledgements

The authors thank the Ministry for Culture and Science of North Rhine Westphalia (Germany) for funding this work within the International Graduate School for Battery Chemistry, Characterization, Analysis, Recycling, and Application (BACCARA). F.D.B., M.M.B., and M.C.S. acknowledge the financial support by the BMBF (Bundesministerium für Bildung und Forschung) within the ProLiFest (03XP0253A) project. In addition, the authors greatly acknowledge Andre Bar for graphics support.

Open access funding enabled and organized by Projekt DEAL.

#### **Conflict of Interest**

The authors declare no conflict of interest.

## **Data Availability Statement**

The data that support the findings of this study are available from the corresponding author upon reasonable request.

#### Keywords

active lithium loss, Li metal, lithium ion batteries, pre-lithiation, silicon thin films

Received: February 6, 2022 Revised: February 23, 2022 Published online: March 22, 2022

- [1] a) T. Placke, R. Kloepsch, S. Dühnen, M. Winter, J. Solid State Electrochem. 2017, 21, 1939; b) E. Adhitama, P. C. Rath, A. Prayogi, J. Patra, T.-C. Lee, J. Li, J.-K. Chang, Carbon 2021, 184, 752.
- [2] a) D. H. S. Tan, Y.-T. Chen, H. Yang, W. Bao, B. Sreenarayanan, J.-M. Doux, w. Li, B. Lu, S.-Y. Ham, B. Sayahpour, J. Scharf, E. A. Wu, G. Deysher, H. E. Han, H. J. Hah, H. Jeong, J. B. Lee, Y. S. Meng, Science 2021, 373, 1494; b) M. Marinaro, D. Bresser, E. Beyer, P. Faguy, K. Hosoi, H. Li, J. Sakovica, K. Amine, M. Wohlfahrt-Mehrens, S. Passerini, J. Power Sources 2020, 459, 228073; c) R. Schmuch, R. Wagner, G. Hörpel, T. Placke, M. Winter, Nat. Energy 2018, 3, 267.
- [3] M. Winter, J. Besenhard, J. Albering, J. Yang, M. Wachtler, in *Progress in Batteries and Battery Materials*, Vol. 17 (Ed: L. Breveglieri), Graz University of Technology, Graz 1998, p. 208.
- [4] P. Meister, H. Jia, J. Li, R. Kloepsch, M. Winter, T. Placke, Chem. Mater. 2016, 28, 7203.
- [5] a) A. F. Gonzalez, N.-H. Yang, R.-S. Liu, J. Phys. Chem. C 2017, 121, 27775; b) T. Placke, G. G. Eshetu, M. Winter, E. Figgemeier, in Lithium-Ion Batteries Enabled by Silicon Anodes, (Eds: C. Ban, K. Xu), The Institution of Engineering and Technology (IET), UK 2021, p. 349; c) S. Dühnen, J. Betz, M. Kolek, R. Schmuch, M. Winter, T. Placke, Small Methods 2020, 4, 2000039.
- [6] a) J. Chen, X. Fan, Q. Li, H. Yang, M. R. Khoshi, Y. Xu, S. Hwang, L. Chen, X. Ji, C. Yang, H. He, C. Wang, E. Garfunkel, D. Su, O. Borodin, C. Wang, Nat. Energy 2020, 5, 386; b) I. Hasa, A. M. Haregewoin, L. Zhang, W.-Y. Tsai, J. Guo, G. M. Veith, P. N. Ross, R. Kostecki, ACS Appl. Mater. Interfaces 2020, 12, 40879; c) U. S. Vogl, S. F. Lux, E. J. Crumlin, Z. Liu, L. Terborg, M. Winter, R. Kostecki, J. Electrochem. Soc. 2015, 162, A603; d) M. Winter, W. K. Appel, B. Evers, T. Hodal, K.-C. Möller, I. Schneider,

- M. Wachtler, M. R. Wagner, G. H. Wrodnigg, J. O. Besenhard, Monatsh. Chem. 2001, 132, 473.
- [7] M. Wachtler, J. O. Besenhard, M. Winter, J. Power Sources 2001, 94, 189
- [8] F. Holtstiege, A. Wilken, M. Winter, T. Placke, Phys. Chem. Chem. Phys. 2017, 19, 25905.
- [9] a) S. Chae, M. Ko, K. Kim, K. Ahn, J. Cho, Joule 2017, 1, 47;
   b) B. Han, X. Li, S. Bai, Y. Zou, B. Lu, M. Zhang, X. Ma, Z. Chang, Y. S. Meng, M. Gu, Matter 2021, 4, 3741.
- [10] a) D. Vrankovic, M. Graczyk-Zajac, C. Kalcher, J. Rohrer, M. Becker, C. Stabler, G. Trykowski, K. Albe, R. Riedel, ACS Nano 2017, 11, 11409; b) H. Wu, G. Zheng, N. Liu, T. J. Carney, Y. Yang, Y. Cui, Nano Lett. 2012, 12, 904; c) W. Wu, Y. Kang, M. Wang, D. Xu, J. Wang, Y. Cao, C. Wang, Y. Deng, J. Power Sources 2020, 464, 228244.
- [11] a) Y. Horowitz, H.-L. Han, F. A. Soto, W. T. Ralston, P. B. Balbuena, G. A. Somorjai, Nano Lett. 2018, 18, 1145; b) A. Schiele, B. Breitung, T. Hatsukade, B. B. Berkes, P. Hartmann, J. Janek, T. Brezesinski, ACS Energy Lett. 2017, 2, 2228; c) G. G. Eshetu, E. Figgemeier, ChemSusChem 2019, 12, 2515.
- [12] a) S. Guo, H. Li, Y. Li, Y. Han, K. Chen, G. Xu, Y. Zhu, X. Hu, Adv. Energy Mater. 2018, 8, 1800434; b) S. Kim, Y. K. Jeong, Y. Wang, H. Lee, J. W. Choi, Adv. Mater. 2018, 30, 1707594; c) N. S. Hochgatterer, M. R. Schweiger, S. Koller, P. R. Raimann, T. Wöhrle, C. Wurm, M. Winter, Electrochem. Solid-State Lett. 2008, 11 A76
- [13] a) F. Holtstiege, P. Bärmann, R. Nölle, M. Winter, T. Placke, Batteries 2018, 4, 4; b) V. L. Chevrier, L. Liu, R. Wohl, A. Chandrasoma, J. A. Vega, K. W. Eberman, P. Stegmaier, E. Figgemeier, J. Electrochem. Soc. 2018, 165, A1129; c) M.-T. F. Rodrigues, J. A. Gilbert, K. Kalaga, D. P. Abraham, J. Phys. Energy 2020, 2, 024002.
- [14] a) R. Zhan, X. Wang, Z. Chen, Z. W. Seh, L. Wang, Y. Sun, Adv. Energy Mater. 2021, 11, 2101565; b) J. Betz, L. Nowak, M. Winter, T. Placke, R. Schmuch, J. Electrochem. Soc. 2019, 166, A3531.
- [15] a) M. G. Scott, A. H. Whitehead, J. R. Owen1, J. Electrochem. Soc. 1998, 145, 1506; b) T. Tabuchi, H. Yasuda, M. Yamachi, J. Power Sources 2005, 146, 507; c) A. Veluchamy, C.-H. Doh, D.-H. Kim, J.-H. Lee, D.-J. Lee, K.-H. Ha, H.-M. Shin, B.-S. Jin, H.-S. Kim, S.-I. Moon, C.-W. Park, J. Power Sources 2009, 188, 574; d) K. Yao, R. Liang, J. P. Zheng, J. Electrochem. Energy Convers. Storage 2016, 13, 011004; e) M.-Y. Yan, G. Li, J. Zhang, Y.-F. Tian, Y.-X. Yin, C.-J. Zhang, K.-C. Jiang, Q. Xu, H.-L. Li, Y.-G. Guo, ACS Appl. Mater. Interfaces 2020, 12, 27202.
- [16] a) H. J. Kim, S. Choi, S. J. Lee, M. W. Seo, J. G. Lee, E. Deniz, Y. J. Lee, E. K. Kim, J. W. Choi, Nano Lett. 2015, 16, 282;
  b) P. K. Nayak, T. R. Penki, B. Markovsky, D. Aurbach, ACS Energy Lett. 2017, 2, 544;
  c) G. M. Overhoff, R. Nölle, V. Siozios, M. Winter, T. Placke, Batteries Supercaps 2021, 4, 1163.
- [17] a) M. W. Forney, M. J. Ganter, J. W. Staub, R. D. Ridgley, B. J. Landi, Nano Lett. 2013, 13, 4158; b) Y. Li, B. Fitch, Electrochem. Commun. 2011, 13, 664; c) P. Bärmann, M. Mohrhardt, J. E. Frerichs, M. Helling, A. Kolesnikov, S. Klabunde, S. Nowak, M. R. Hansen, M. Winter, T. Placke, Adv. Energy Mater. 2021, 11, 2100925; d) Q. Meng, G. Li, J. Yue, Q. Xu, Y.-X. Yin, Y.-G. Guo, ACS Appl. Mater. Interfaces 2019, 11, 32062.
- [18] J. Guo, D. Dong, J. Wang, D. Liu, X. Yu, Y. Zheng, Z. Wen, W. Lei, Y. Deng, J. Wang, G. Hong, H. Shao, Adv. Funct. Mater. 2021, 31, 2102546.
- [19] a) Z. Wang, Y. Fu, Z. Zhang, S. Yuan, K. Amine, V. Battaglia, G. Liu, J. Power Sources 2014, 260, 57; b) B. B. Fitch, M. Yakovleva, Y. Li, I. Plitz, A. Skrzypczak, F. Badway, G. G. Amatucci, Y. Gao, ECS Trans. 2007, 3, 15.
- [20] B. E. Conway, W. G. Pell, T.-C. Liu, J. Power Sources 1997, 65, 53.
- [21] J. O. M. Besenhard, M. Winter, J. Yang, W. Biberacher, J. Power Sources 1995, 54, 228.



www.advancedsciencenews.com www.afm-journal.de

ADVANCED FUNCTIONAL MATERIALS

- [22] I. Cekic-Laskovic, N. von Aspern, L. Imholt, S. Kaymaksiz, K. Oldiges, B. R. Rad, M. Winter, Top. Curr. Chem. 2017, 375, 37.
- [23] A. R. Jiménez, R. Nölle, R. Wagner, J. Hüsker, M. Kolek, R. Schmuch, M. Winter, T. Placke, *Nanoscale* 2018, 10, 2128.
- [24] Z. Liang, D. Lin, J. Zhao, Z. Lu, Y. Liu, C. Liu, Y. Lu, H. Wang, K. Yan, X. Tao, Y. Cui, Proc. Natl. Acad. Sci. USA 2016, 113, 2862.
- [25] W. Plieth, Electrochemistry for Materials Science, Elsevier, Amsterdam 2008.
- [26] R. E. Ruther, K. A. Hays, S. J. An, J. Li, D. L. Wood, J. Nanda, ACS Appl. Mater. Interfaces 2018, 10, 18641.
- [27] T. Gruber, D. Thomas, C. Röder, F. Mertens, J. Kortus, J. Raman Spectrosc. 2013, 44, 934.
- [28] S.-K. Otto, T. Fuchs, Y. Moryson, C. Lerch, B. Mogwitz, J. Sann, J. Janek, A. Henss, ACS Appl. Energy Mater. 2021, 4, 12798.
- [29] a) C. Cao, I. I. Abate, E. Sivonxay, B. Shyam, C. Jia, B. Moritz, T. P. Devereaux, K. A. Persson, H.-G. Steinrück, M. F. Toney, *Joule* 2019, 3, 762; b) R. Alfonsetti, L. Lozzi, M. Passacantando, P. Picozzi, S. Santucci, *Appl. Surf. Sci.* 1993, 70, 222.
- [30] J. Danet, T. Brousse, K. Rasim, D. Guyomard, P. Moreau, Phys. Chem. Chem. Phys. 2010, 12, 220.
- [31] M. N. Obrovac, L. Christensen, Electrochem. Solid-State Lett. 2004, 7, A93.
- [32] a) M. Winter, K.-C. Möller, J. Besenhard, in *Lithium Batteries: Science and Technology*, (Eds: G. A. Nazri, G. Pistoia), Kluwer Academic

- Publisher, New York **2004**, p. 144; b) M. Winter, J. O. Besenhard, in *Lithium Ion Batteries-Fundamentals and Performance*, (Eds: M. Wakihara, O. Yamamoto), Wiley, Tokyo **1998**, p. 127.
- [33] F. Sagane, K.-i. Ikeda, K. Okita, H. Sano, H. Sakaebe, Y. Iriyama, J. Power Sources 2013, 233, 34.
- [34] Y. Jiang, G. Offer, J. Jiang, M. Marinescu, H. Wang, J. Electrochem. Soc. 2020, 167, 130533.
- [35] a) M. T. McDowell, S. W. Lee, W. D. Nix, Y. Cui, Adv. Mater. 2013, 25, 4966; b) M. N. Obrovac, V. L. Chevrier, Chem. Rev. 2014, 114, 11444.
- [36] M. Petzl, M. A. Danzer, J. Power Sources 2014, 254, 80.
- [37] J. Li, J. R. Dahn, J. Electrochem. Soc. 2007, 154, A156.
- [38] D. S. M. Iaboni, M. N. Obrovac, J. Electrochem. Soc. 2015, 163, A255.
- [39] Y. Yin, E. Arca, L. Wang, G. Yang, M. Schnabel, L. Cao, C. Xiao, H. Zhou, P. Liu, J. Nanda, G. Teeter, B. Eichhorn, K. Xu, A. Burrell, C. Ban, ACS Appl. Mater. Interfaces 2020, 12, 26593.
- [40] L. Y. Beaulieu, K. W. Eberman, R. L. Turner, L. J. Krause, J. R. Dahn, Electrochem. Solid-State Lett. 2001, 4, A137.
- [41] A. R. Jiménez, R. Klöpsch, R. Wagner, U. C. Rodehorst, M. Kolek, R. Nölle, M. Winter, T. Placke, ACS Nano 2017, 11, 4731.
- [42] a) M. K. Datta, P. N. Kumta, J. Power Sources 2009, 194, 1043;
   b) M. N. Obrovac, L. J. Krause, J. Electrochem. Soc. 2007, 154, A103.
- [43] J. O. Besenhard, M. W. Wagner, M. Winter, A. D. Jannakoudakis, P. D. Jannakoudakis, E. Theodoridou, J. Power Sources 1993, 44, 413.
- [44] R. Nölle, K. Beltrop, F. Holtstiege, J. Kasnatscheew, T. Placke, M. Winter, Mater. Today 2020, 32, 131.